Electronic Supplementary Material

^{40}Ar–^{39}Ar dating of volcanogenic products from the AND-2A core (ANDRILL Southern McMurdo Sound Project, Antarctica): correlations with the Erebus Volcanic Province and implications for the age model of the core

by

G. Di Vincenzo, L. Bracciali, P. Del Carlo, K. Panter, S. Rocchi

1. Methods

Sample preparation and ^{40}Ar–^{39}Ar data collection were completed at IGG–CNR, Pisa (Italy). Samples selected for ^{40}Ar–^{39}Ar dating before processing, that is as received at IGG–CNR laboratory, are shown in Fig. S1. Samples affected by alteration, evident under the optical or electronic microscope, were rejected and not analyzed.

Polished thin sections from each sample were investigated by a light microscope and by scanning electron microscopy (SEM) using a Philips XL30 (using an accelerating voltage of 20 kV, sample current of 10 nA and 0.5 μm beam diameter) equipped with an energy dispersive system (EDS) at the Dipartimento di Scienze della Terra, Pisa.

After crushing and sieving, groundmasses and feldspars (plagioclase or alkali feldspar) were concentrated from different grain sizes (see Tables S1) using standard separation techniques, and further purified by hand-picking under a stereomicroscope. Groundmass separates were leached in an ultrasonic bath (heated to ~50°C) for 1 h in HCl 3.5 N and 1h in HNO_3 1N (Koppers et al. 2000). Feldspars were leached at room temperature in an ultrasonic bath for a few minutes. A longer leaching time (20 min) was used for alkali feldspar 8.88–9.02 mbsf, because of the presence of melt inclusions. After leaching, samples were washed in ultraclean water and dried on a hot plate at ~70°C. Splits of a few to several tens of milligrams of feldspars and groundmasses were wrapped in aluminium foil to form discs <9 mm in diameter and a few millimetres thick. Discs were stacked in pancake fashion within a quartz vial 9 mm in diameter. The stack was interspersed with splits of the standard Fish Canyon sanidine (FCs), every 4–6 mm to monitor the vertical neutron flux. *J* values for each stack position were monitored by analyzing 5 single crystals of FCs (assumed age 28.03 Ma, Jourdan and Renne 2007). Samples were irradiated in three distinct batches, for 5 h (PAV–64), 2 h (PAV–65) and 3 h (PAV–66), in the core of the TRIGA reactor at the University of Pavia (Italy). ^{40}Ar–^{39}Ar analyses were carried out using different laser extraction techniques and different laserprobes: (1) laser total fusion analysis of single or multi-grain splits of K-rich alkali feldspar using a CO_2 laser; (2) laser step-heating analysis using either a defocused Nd-doped yttrium-aluminium-garnet (Nd:YAG) laser (for groundmasses) or a defocused CO_2 laser (feldspars). After irradiation, splits consisting of one to a few grains of alkali feldspars (a few milligrams for total fusion analyses to a few tens of milligrams for step-heating analysis were used only for sample 8.88–9.02 mbsf) to a few tens of milligrams for plagioclase and groundmasses, were placed in 1.5- to 9-mm diameter holes (depending on the sample mass) of a copper holder and baked overnight. Total fusion analyses on alkali feldspars (including the fluence monitor FCs) were carried out using a continuous wave CO_2 laser defocused to 1 mm spot size. Step-heating analyses of groundmasses were performed using a continuous wave diode-pumped Nd:YAG laser, which was defocused to a 2 mm spot size and slowly rastered (at 0.1 mm s^{-1}) over the grains by a computer-controlled x–y stage to ensure even heating. One plagioclase and one alkali feldspar concentrates were incrementally heated using the CO_2 laser defocused to 3 mm spot size, which was manually rastered over the

grains to ensure even heating. Step-heating analyses were preceded by a total fusion analysis of mg-splits of the same separate in order to estimate a preliminary age then used to calculate the optimal sample weight for the step-heating run.

After cleanup (8–10 min, including 1 min of lasering for total fusion analyses and 15–20 min for step-heating experiments, including 8–9 min of lasering), using two Saes AP10 getters held at 400°C and one C–50 getter held at room temperature, extracted gases were equilibrated by automated valves into a MAP215–50 noble gas mass spectrometer fitted with a Balzers SEV217 secondary electron multiplier. Ar isotope peak intensities were measured ten times for a total of ~25 min. Blanks were analyzed every one to three analyses. Mass discrimination was monitored by analysis of air pipettes. At the time of data collection mean values were: 1.0051±0.0030 (±2SD, n=33) per atomic mass unit (AMU) for PAV–64, 1.0037±0.0016 (±2SD, n=13) AMU for PAV–65, and 1.0038±0.0018 (±2SD, n=22) AMU for PAV–66. Correction factors for interfering isotopes, determined on K- and Ca-rich glasses, were: $(^{40}Ar/^{39}Ar)_K$=0.0093, $(^{38}Ar/^{39}Ar)_K$=0.0129, $(^{39}Ar/^{37}Ar)_{Ca}$=0.00075 and $(^{36}Ar/^{37}Ar)_{Ca}$=0.00024. Data reduction was performed using the ArArCALC software (Koppers, 2002). Errors are given at 2σ and are quoted as: (1) analytical errors, including in-run statistics and uncertainties in the discrimination factor, interference corrections and procedural blanks; (2) internal errors, also including uncertainties in the *J* value; (3) full errors, also including uncertainties on the age of the flux monitor and those in the ^{40}K decay constants. Data corrected for post-irradiation decay, mass discrimination effects, isotopes derived from interference reactions and blanks are listed in Table S1. Ages listed in Table S1 were calculated using the IUGS recommended constants (Steiger and Jäger 1977). More details on the analytical procedures can be found in Di Vincenzo and Skála (2009). Error-weighted means and least squares fits were calculated using v. 3.00 of the Isoplot/Ex program (Ludwig 2003).

2. Features of dated rocks

Lithostratigraphic Unit 1 (0 – 37.01 mbsf)

Five samples, consisting of vesiculated lava clasts up to a few centimetres in size, were selected from the Lithostratigraphic Unit 1. A comprehensive description of these samples have been reported by Del Carlo et al. (2009) and will be only summarized here. Sample 8.88–9.02 (a fresh phonolite lava, Fig. S2a) is a lava clast that belongs to the first interval of the core recovered as loose samples in composite bags (bagged samples, i.e. the stratigraphic relationships are not recognizable). It is a fresh subangular glomeroporphyritic lava clast of phonolitic composition containing cm-sized anhedral anorthoclase (Fig. S3) phenocrysts with large glass inclusions (up to 0.5 mm), subhedral medium-grained phenocrysts of zoned clinopyroxene and minor olivine, set in an almost opaque glassy vesiculated groundmass. Flattened vesicles and elongated phenocrysts define a flowage texture.

Sample 10.22–10.44 is a variably vesiculated (5–20%) basanitic lava clast (Fig. S2b) characterized by a phenocrystic assemblage of euhedral skeletal olivine up to 4 mm in length and minor clinopyroxene in a brown glassy groundmass with microlites of clinopyroxene, plagioclase and oxides. Vesicles are irregular in shape and the groundmass consists of patches and streaks of a black to almost opaque glass (i.e., tachylite).

Sample 12.23–12.41 is a glomeroporphyritic vesiculated hawaiitic lava clast characterized by phenocrysts of zoned clinopyroxene (pale-green core to purple-brown rim) and minor olivine in a glassy groundmass that includes microlites of plagioclase, clinopyroxene and magnetite (Fig. S2c). The millimeter-sized rounded vesicles are partially filled with secondary calcite.

The hawaiitic lava clast 18.03–18.25 contains rounded vesicles and phenocrysts of zoned clinopyroxene and minor altered olivine in a glassy groundmass that includes microlites of clinopyroxene, plagioclase and oxides (Fig. S2d).

Sample 18.69–18.73 is a vesiculated (20%) lava clast with a subrounded shape. It is tephritic in composition and contains phenocrysts of clinopyroxene and minor bowlingitic olivine (Fig. S2e).

Lithostratigraphic Unit 4 (122.86 – 224.82 mbsf)

Samples 127.50–127.52 and 129.96–129.97 are two clasts from a diamictite, which is the main lithofacies of Lithostratigraphic Unit 4 (Fielding et al. 2008).

Sample 127.50–127.52 is 1 x 2 centimeter-sized subangular lava clast, consisting of a subaphyric trachyte (Fig. S2f) with scattered anorthoclase (Fig. S3) and green pyroxene microphenocrysts set in a trachytic-textured groundmass made of alkali feldspars and magnetite.

Sample 129.96–129.97 is a 1 x 3 centimeter-sized subangular porphyritic (15 vol%) basaltic lava clast with ~1 mm-sized phenocrysts of plagioclase, clinopyroxene and olivine pseudomorphs. The groundmass is made up of plagioclase microlites, altered glass and minor opaque minerals (Fig. S2g).

Lithostratigraphic Unit 7 (339.92 – 436.18 mbsf)

Sample 358.11–358.13 is a purplish to dark-brown, a few centimeters wide lava clast from a diamictite level. Euhedral magnetite phenocrysts and tiny plagioclase microphenocrysts, which define a pilotaxitic texture, are set in a holocrystalline groundmass with plagioclase, clinopyroxene, magnetite and apatite (Fig. S2h).

Lithostratigraphic Unit 8 (436.18 – 607.35)

Sample 440.83-440.86 is a 5 x 4 centimeter-sized, dark-brown to red, vesicular (15–20 vol%), poorly porphyritic (<1%), intermediate lava clast from a mudstone layer, with

microphenocrysts of plagioclase, abundant magnetite and alkali feldspar in a moderately altered holocrystalline groundmass (Fig. S2i).

Sample 564.92–564.93 is a grey, non-vesicular, porphyritic (10-15 vol%) felsic lava clast from a sandy conglomerate, with phenocrysts of alkali feldspar (~10 vol%), aegirinic clinopyroxene and minor magnetite set in a fine-grained holocrystalline groundmass. The groundmass contains plagioclase, alkali feldspar (mainly anorthoclase in composition, Fig. S3), clinopyroxene and magnetite.

Lithostratigraphic Unit 9 (607.35 – 648.74 mbsf)

Sample 640.13–640.16 belongs to a six-centimeter thick normally graded primary pyroclastic deposit within a sandstone interval and consists of grayish fine pumice lapilli to coarse ash. The pumice clasts are aphyric but in rare instances contain phenocrysts of alkali feldspar (mainly anorthoclase in composition, Fig. S3), the latter commonly found as isolated crystal fragments crystals up to ~0.5 mm in size (Fig. S2k). The pumice have very low alkali, magnesium and iron content pointing to a high degree of alteration (Panter et al., 2008). Pumice from the lapilli tuff are set in a fine-grained matrix of volcanic ash of the same chemical composition. Rare siliciclastic fragments (rounded quartz and lithic fragments) are also found. These observations, coupled with the gradational top and the loaded base of the layer, suggest that the deposit formed by direct sinking of a subaerial pyroclastic fallout (Panter et al., 2008).

Lithostratigraphic Unit 10 (648.74 – 778.34 mbsf)

Sample 709.14–709.16 and 709.17–709.19 are two similar ~3.5-cm thick layers made of rounded fine pumice lapilli, concentrated along ripple foresets. Pumice are subaphyric (with rare anorthoclase phenocrysts, Fig. S3) whose variably flattened vesicles are filled with calcite (Fig. S2l). Within the pumice clasts a significant amount of foreign detritus is present. Subangular to angular monomineralic clasts (up to ~0.3 mm in size) are represented by quartz, plagioclase, minor microcline and subordinate biotite and amphibole. The lithic component is dominated by volcanic clasts (orange-brownish, vesiculated sideromelane, minor tachylite and holocrystalline very fine-grained holocrystalline porphyritic lava). On the basis of lithological features, these deposits are interpreted as two pyroclastic fall events that settled through the water column to the seafloor and were then reworked by shallow water, wave-base processes.

Lithostratigraphic Unit 11 (778.34 – 904.66 mbsf)

Sample 831.66–831.68 represents the thickest (~1 cm thick) of three intervals in Lithostratigraphic Unit 11, where pumice clasts are concentrated. This clast-rich layer, in which the main component is represented by up to 4 mm-sized pumice, has gradational top and bottom contacts within a silty sandstone, which indicates a very weak reworking of a

pyroclastic fall deposit. Monomineralic fragments (alkali feldspar, plagioclase and minor quartz) along with lithic (mostly porphyritic volcanic) clasts also occur (Fig. S2m).

Lithostratigraphic Unit 12 (904.66 – 996.69 mbsf)

The analyzed samples from Lithostratigraphic Unit 12 represent two out of the six accumulations ranging from 2 to 10 cm thick (from the 953–964-mbsf interval) of yellow-grey pumices mixed with dark green highly angular clasts dispersed in a muddy fine-grained sandstone. The pumiceous layer of sample 953.28–953.31 (Fig. S2n) is made up of medium- to coarse-grained pumice fragments and also contains single crystals of euhedral anorthoclase (commonly broken) (Fig. S3), subordinate quartz and plagioclase as well as porphyritic pilotaxitic fragments (up to 1–2 mm sized). In sample 953.54–953.56, which is similar in overall composition to the former, pumices are concentrated in a ~1 cm-thick irregular strip and the amount of monomineralic sialic fragments is lower. Pumice are more altered with respect to those of the previous deposits, nevertheless the lack of foreign detritus in the matrix indicates that the pumice accumulations represent nearly primary tephra layers formed by pyroclastic activity.

Lithostratigraphic Unit 14 (1040.28 – 1138.54 mbsf)

The lowermost lithostragraphic unit consists of sandy diamictite and sandstone with dispersed clasts. Sample 1093.00–1093.04 was taken from a 6 cm-thick interval pumice-rich layer that shows sharp, highly angular to crenulated contacts with the surrounding sandstone. It is formed of dense non-vesicular glassy lense-shaped pumice clasts, subangular fresh monomineralic fragments [anorthoclase (Fig. S3), quartz and plagioclase] and felty to pilotaxitic textured volcanic clasts (Fig. S2o). The dark colour of the sample is due to the almost opaque matrix. Individual pumice are altered and replaced similarly to sample 953.54–953.56 and vary in colour from black to dark-green to brown. This layer is mostly matrix-supported, however, there are local areas where lense-shaped pumices are in contact and are imbricated. Foreign detritus is scarce. On the basis of the described features, this deposit represents a pyroclastic event that was very weakly reworked and later intruded by intra-formational sands (e.g., clastic dike-like).

References

Del Carlo P, Panter KS, Bassett K, Bracciali L, Di Vincenzo G, Rocchi S. (2009) Evidence for local volcanic sources in the upper lithostratigraphic unit of ANDRILL AND-2A core (Southern McMurdo Sound, Antarctica) and implications for paleoenvironment and subsidence in the western Victoria Land basin. Global Planet Change. doi: 10.1016/jgloplacha.2009.09.002

Di Vincenzo G, Skála R (2009) ^{40}Ar–^{39}Ar laser dating of tektites from the Cheb Basin (Czech republic): Evidence for coevality with moldavites and influence of the dating standard on the age of the Ries impact. Geochim Cosmochim Acta, 73:493–513

Fielding CR, Atkins CB, Bassett KN, Browne GH, Dunbar GB, Field BD, Frank TD, Panter KS, Pekar SF, Krissek LA, Passchier S (2008) Sedimentology and stratigraphy of the AND-2A core, ANDRILL Southern McMurdo Sound, Project, Antarctica. In: Harwood DM, Florindo F, Talarico F, Levy RH (eds), Studies from the ANDRILL, Southern McMurdo Sound Project, Antarctica. Terra Antarctica, 15 (in press)

Jourdan F, Renne PR (2007) Age calibration of the Fish Canyon sanidine $^{40}Ar/^{39}Ar$ dating standard using primary K–Ar standard. Geochim Cosmochim Acta 71:387–402

Koppers AAP (2002) ArArCALC—software for $^{40}Ar/^{39}Ar$ age calculations. Comp Geosci 28:605–619

Koppers AAP, Staudigel H, Wijbrans JR (2000) Dating crystalline groundmass separates of altered Cretaceous seamount basalts by the $^{40}Ar/^{39}Ar$ incremental heating technique. Chem Geol 166:139–158

Ludwig KR (2003) User's manual for Isoplot 3.00, a geochronological toolkit for Microsoft Excel. Berkeley Geochronology Center Spec Pub, 4:54 pp

Panter KS, Talarico F, Bassett K, Del Carlo P, Field B, Frank T, Hoffman S, Kuhn G, Reichelt L, Sandroni S, Tavini M, Bracciali L, Cornamusini G, von Eynatten H, Rocchi R (2008) Petrologic and Geochemical Composition of the AND-2A Core, ANDRILL Southern McMurdo Sound Project, Antarctica. In: Harwood DM, Florindo F, Talarico F, Levy RH (eds), Studies from the ANDRILL, Southern McMurdo Sound Project, Antarctica. Terra Antarctica, 15 (in press)

Steiger RH, Jäger E (1977) Subcommission on Geochronology: convention on the use of decay constants in geo- and cosmochronology. Earth Planet Sci Lett 36:359–362

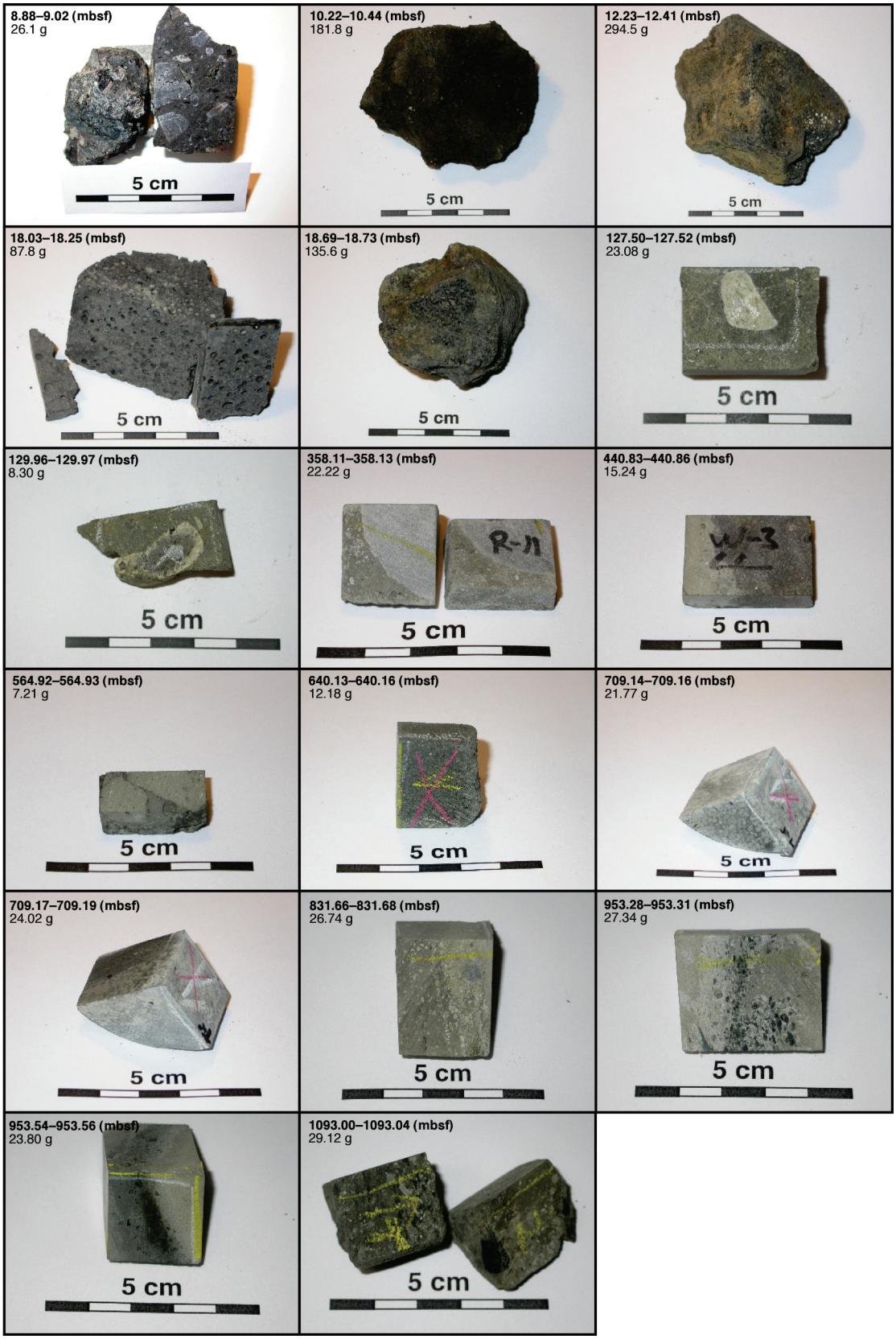

Fig. S1 Photographs showing samples selected for ^{40}Ar–^{39}Ar dating before processing.

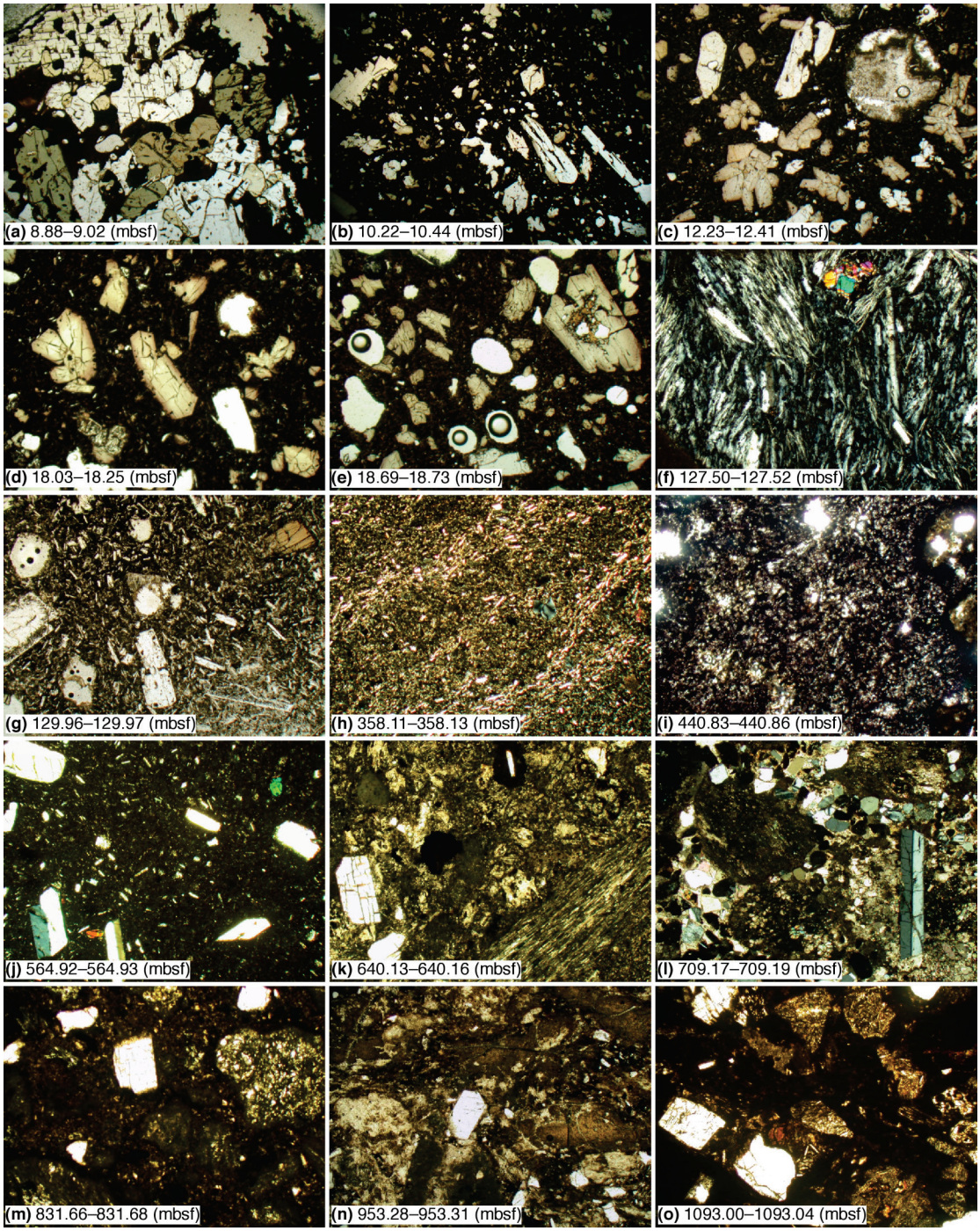

Fig. S2 Microphotographs showing the main petrographical features of samples selected for ^{40}Ar–^{39}Ar dating from the AND-2A core. **a** sample 8.88–9.02, phonolite lava clast with phenocrysts of coarse-grained alkali feldspar, medium-grained pale-green clinopyroxene and minor yellowish olivine set in an almost opaque groundmass, plane polarized light (PPL), field of view 5.5 mm. **b** sample 10.22–10.44, basanite lava clast with a phenocrystic assemblage of euhedral skeletal olivine and minor pale-brown clinopyroxene in a dark brown glassy groundmass, PPL, field of view 6 mm. **c** sample 12.23–12.41, hawaiite lava clast with glomeroporphyritic clusters of zoned (pale-green core to purple brown rim) clinopyroxene and minor olivine; the rounded vesicle (top-right of image) is partially filled with secondary calcite; PPL, field of view 3 mm. **d** sample 18.03–18.25, hawaiite lava clast with phenocrysts of zoned clinopyroxene and minor altered olivine in a glassy groundmass, PPL, field of view 3 mm. **e** sample 18.69–18.73, vesiculated tephrite lava clastcontaining phenocrysts of clinopyroxene and minor bowlingitic olivine; note the piroxene with a glassy core (top-right corner of image), PPL, field of view 5 mm. **f** sample 127.50–127.52, trachyte lava clast, with scattered alkali feldspar and minor green pyroxene (top-center) microphenocrysts set in a trachytic-textured groundmass made of alkali feldspars and magnetite, crossed polarized light (CPL), field of view 2 mm. **g** sample 129.96–129.97, basaltic lava clast with phenocrysts of plagioclase, clinopyroxene (top-right) and olivine pseudomorphs (center of

image), PPL, field of view 4 mm. **h** sample 358.11–358.13, euhedral magnetite phenocrysts and tiny plagioclase microphenocrysts define a pilotaxitic alignment in this basaltic lava clast, CPL, field of view 5.5 mm. **i** sample 440.83–440.86, vesicular poorly porphyritic intermediate lava clast with microphenocrysts of plagioclase, abundant magnetite and minor alkali feldspar in a moderately altered holocrystalline groundmass, PPL, field of view 3 mm. **j** sample 564.92–564.93, felsic lava clast with euhedral phenocrysts of alkali feldspar, aegirinic clinopyroxene and minor magnetite, CPL, field of view 5.5 mm. **k** sample 640.13–640.16, pyroclastic deposit containing angular vesiculated pumices (bottom-right of image), rarely with phenocrysts of alkali feldspar, the latter commonly found as isolated crystal fragments crystals (left of image), PPL, field of view 3 mm. **l** sample 709.17–709.19, coarse-grained pumiceous sandstone with a carbonatic cement found within a pumice- rich layer, note the three subaphyric pumices and the alkali feldspar (right), CPL, field of view 3 mm. **m** sample 831.66–831.68, pumice- rich layer with subordinate monomineralic feldspars grains, PPL, field of view 3 mm. **n** sample 953.28–953.31, pumiceous layer containing monomineralic euhedral alkali feldspar grains (e.g. center of image), PPL, field of view 3 mm. **o** sample 1093.00–1093.04, blocky dense clast, dark due to the almost opaque matrix, with strongly altered pumices, subangular fresh monomineralic felspars and quartz fragments and felty to pylotaxitic textured volcanic clasts, PPL, field of view 6 mm.

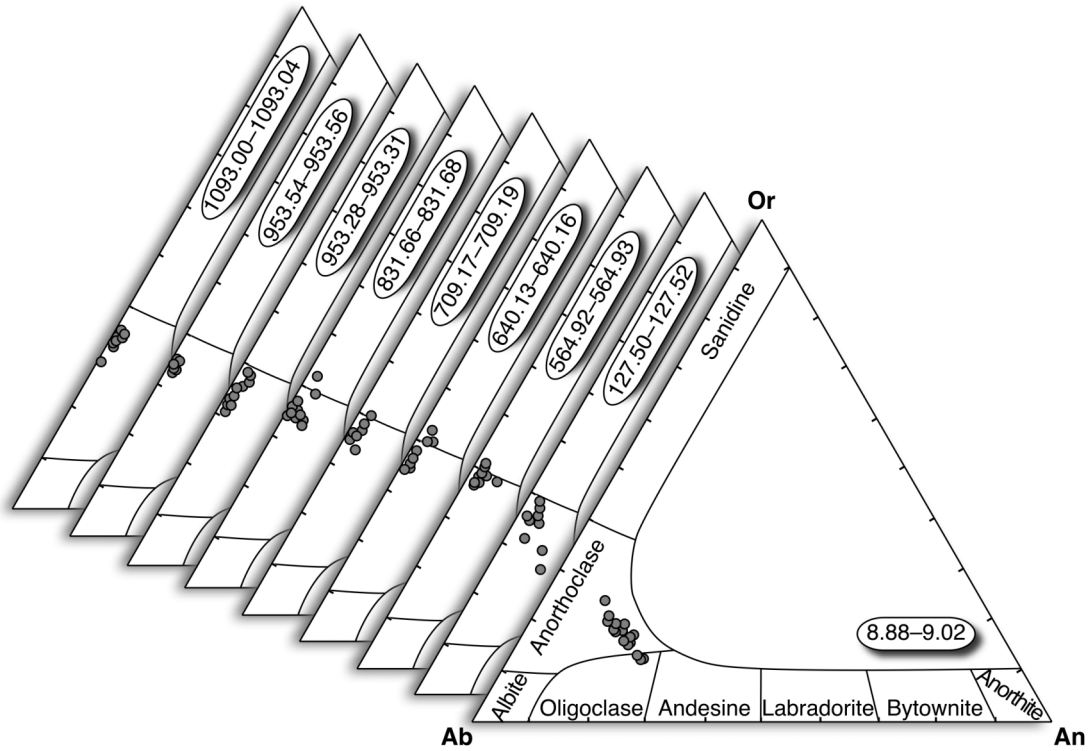

Fig. S3 K-feldspar–Albite–Anorthite triangular plot showing the compositions of alkali feldspars analyzed by the ^{40}Ar–^{39}Ar method.

Table S1 ^{40}Ar–^{39}Ar data of groundmasses and feldspars from volcanic samples of the AND-2A Core (ANDRILL SMS Project). Argon isotope concentrations are $x10^{-15}$ moles.

No.	weight (mg) laser power (W) # grains	$^{36}Ar_{(atm)}$	$^{37}Ar_{(Ca)}$	$^{38}Ar_{(Cl)}$	$^{39}Ar_{(K)}$	$^{40}Ar_{(Tot)}$	Age (Ma)	±2σ	$^{40}Ar^*$ %	$^{39}Ar_K$ %	Ca/K	±2σ
sample 8.88–9.02, anorthoclase grain size 0.30–0.50 mm, irradiation PAV–65, J=0.0001874±0.0000010												
Total fusion data data												
*1	3.5 mg	0.01440	1.000	0.00301	1.769	4.827	0.109	0.045	11.8	6.4	1.067	0.060
*2	8.2 mg	0.05453	3.382	0.01481	6.492	18.51	0.125	0.028	12.9	23.7	0.983	0.055
*3	7.0 mg	0.03000	2.543	0.01881	4.771	10.56	0.120	0.022	16.0	17.4	1.006	0.056
*4	8.3 mg	0.09283	3.278	0.01990	6.222	29.91	0.135	0.025	8.3	22.7	0.994	0.056
Total gas age							0.125	0.014				
Error-weighted mean age (4 of 4 steps), MSWD=0.59							0.124	0.014				
isochron age ($^{36}Ar/^{40}Ar$ vs. $^{39}Ar/^{40}Ar$ diagram), MSWD=0.89							0.107	0.039				
$^{40}Ar/^{36}Ar$ intercept							301	11				
sample 8.88–9.02, anorthoclase grain size 0.30–0.50 mm, 56.3 mg, irradiation PAV–65, J=0.0001874±0.0000010												
step-heating data												
1	0.3 W	0.32478	0.609	0.00511	1.382	96.28	0.08	0.35	0.3	3.1	0.832	0.048
2	0.5 W	0.02805	0.782	0.00433	1.428	8.831	0.128	0.094	6.1	3.2	1.033	0.059
3	0.8 W	0.02927	2.243	0.01265	4.113	9.293	0.053	0.022	6.9	9.2	1.029	0.058
4	1.3 W	0.02183	2.799	0.01840	5.337	8.298	0.117	0.014	22.1	11.9	0.990	0.056
5	2.0 W	0.04597	4.388	0.04982	8.624	18.87	0.207	0.013	27.9	19.2	0.960	0.054
6	2.8 W	0.02128	2.243	0.02283	4.313	9.095	0.220	0.026	30.7	9.6	0.981	0.055
7	4.1 W	0.00568	1.554	0.00975	2.893	2.979	0.152	0.022	43.3	6.4	1.013	0.058
8	6.6 W	0.00527	4.550	0.00435	8.244	3.857	0.094	0.013	58.4	18.4	1.041	0.058
9	8.0 W	0.01081	4.685	0.00482	8.460	5.047	0.074	0.011	36.2	18.8	1.045	0.058
10	10 W	0.00557	0.05867	bdl	0.09904	1.661	0.05	0.65	0.8	0.2	1.12	0.13
Total gas age							0.127	0.013				
Error-weighted mean age, no plateau							–	–				
sample 10.22–10.44, groundmass, grain size 0.30–0.50 mm, 50.4 mg, irradiation PAV–64, J=0.0004490±0.0000040												
step-heating data												
1	0.20 W	0.01617	0.1139	0.04020	0.1515	5.318	2.9	2.8	10.1	0.2	1.42	0.18
2	0.50 W	0.02453	2.167	0.8095	3.489	11.34	0.95	0.15	36.0	5.6	1.172	0.071
*3	0.70 W	0.01130	3.031	1.132	5.214	8.069	0.735	0.080	58.3	8.4	1.097	0.067
*4	0.90 W	0.01139	3.011	1.058	5.116	7.716	0.689	0.085	56.0	8.3	1.110	0.068
*5	1.2 W	0.4278	6.665	1.772	9.128	134.5	0.72	0.19	6.0	14.8	1.378	0.083
*6	1.5 W	0.1180	16.16	3.238	17.60	49.51	0.674	0.050	29.5	28.4	1.73	0.10
7	1.8 W	0.01514	16.74	1.579	9.013	11.08	0.594	0.035	59.2	14.6	3.50	0.21
8	2.5 W	0.01662	32.72	1.165	6.725	9.387	0.539	0.073	47.4	10.9	9.18	0.56
9	5.5 W	0.02198	96.49	0.7726	4.626	9.229	0.48	0.26	29.5	7.5	39.4	2.4
10	15 W	0.00925	45.40	0.1383	0.8167	2.990	0.25	0.77	8.5	1.3	104.9	6.5
Total gas age							0.662	0.042				
Error-weighted mean age (4 out of 10 steps), MSWD=0.59							0.692	0.038		59.9		
isochron age ($^{36}Ar/^{40}Ar$ vs. $^{39}Ar/^{40}Ar$ diagram), MSWD=0.89							0.691	0.047				
$^{40}Ar/^{36}Ar$ intercept							295.7	5.5				
sample 12.23–12.41, groundmass, grain size 0.30–0.50 mm, 52.1 mg, irradiation PAV–64, J=0.0004524±0.0000039												
step-heating data												
1	0.20 W	0.03455	0.1329	0.04024	0.1656	10.50	1.4	2.7	2.8	0.8	1.51	0.16
2	0.50 W	0.1205	3.773	0.5334	3.390	40.88	1.27	0.30	12.9	16.0	2.10	0.13
*3	0.70 W	0.03368	5.422	0.4906	3.328	13.13	0.78	0.10	24.2	15.7	3.07	0.19

Table S1 Continued

No.	# grains weight (mg) laser power (W)	$^{36}Ar_{(atm)}$	$^{37}Ar_{(Ca)}$	$^{38}Ar_{(Cl)}$	$^{39}Ar_{(K)}$	$^{40}Ar_{(Tot)}$	Age (Ma)	±2σ	$^{40}Ar^{*}$ %	$^{39}Ar_{K}$ %	Ca/K	±2σ
*4	0.90 W	0.02401	5.292	0.5356	3.729	10.76	0.801	0.080	33.9	17.6	2.68	0.16
5	1.2 W	0.03069	4.229	0.5670	3.714	11.96	0.634	0.078	24.1	17.6	2.15	0.14
6	1.5 W	0.03297	7.308	0.4157	2.643	11.95	0.68	0.15	18.5	12.5	5.22	0.32
7	1.8 W	0.02577	19.31	0.3731	2.319	9.026	0.50	0.19	15.6	11.0	15.7	1.0
8	2.5 W	0.01595	30.39	0.2187	1.249	5.219	0.33	0.37	9.6	5.9	45.9	2.8
9	5.0 W	0.01256	58.68	0.07965	0.4316	3.834	0.2	1.7	3.2	2.0	257	17
10	15 W	0.01204	69.03	0.02714	0.1709	3.649	0.4	5.7	2.5	0.8	762	69
Total gas age							0.758	0.090				
Error-weighted mean age, no plateau							*0.793*	*0.062*		*33.4*		
sample 18.03–18.25, groundmass, grain size 0.30–0.50 mm, 1.6 mg, irradiation PAV–64, J=0.0004551±0.0000032												
Total fusion data												
1	15 W	0.4074	9.471	0.1034	0.6397	133.2	16.1	2.2	9.6	–	27.9	1.8
sample 18.69–18.73, groundmass, grain size 0.30–0.50 mm, 2.5 mg, irradiation PAV–64, J=0.0004579±0.0000028												
Total fusion data												
1	15 W	0.5748	8.960	0.3159	1.655	189.2	9.5	1.2	10.2	–	10.21	0.64
sample 127.50–127.52, alkali feldspar, grain size >0.25 mm, irradiation PAV–64, J=0.0004590±0.0000028												
Total fusion data												
*1	1	0.00688	0.04639	bdl	1.952	28.76	11.30	0.15	92.9	3.8	0.0448	0.0070
*2	1	0.02792	0.50067	0.00272	9.131	133.7	11.345	0.049	93.8	17.7	0.1035	0.0058
*3	1	0.00353	0.13080	0.00026	5.087	71.10	11.368	0.069	98.5	9.9	0.0485	0.0030
*4	2	0.00240	0.09199	0.00044	4.365	60.91	11.385	0.071	98.8	8.5	0.0398	0.0028
*5	3	0.00333	0.13593	bdl	3.567	49.99	11.341	0.080	98.0	6.9	0.0719	0.0049
*6	5	0.00463	0.08861	0.00033	2.731	38.70	11.284	0.096	96.4	5.3	0.0612	0.0040
*7	1	0.01299	0.15140	bdl	5.419	78.34	11.350	0.069	95.0	10.5	0.0527	0.0032
*8	1	0.02048	0.11028	0.00022	3.807	58.32	11.334	0.096	89.6	7.4	0.0547	0.0039
9	3	0.03539	0.11703	0.00042	3.217	55.38	11.53	0.11	81.1	6.3	0.0686	0.0047
*10	7	0.00140	0.03789	bdl	1.313	18.50	11.37	0.19	97.7	2.6	0.0544	0.0078
*11	5	0.00328	0.02601	0.00069	0.9377	13.78	11.27	0.26	92.9	1.8	0.052	0.010
*12	1	0.01629	0.23925	0.00416	9.924	142.0	11.414	0.048	96.5	19.3	0.0455	0.0034
Total gas age							11.369	0.072				
Error-weighted mean age (11 of 12 runs), MSWD=1.65							11.363	0.072				
isochron age ($^{36}Ar/^{40}Ar$ vs. $^{39}Ar/^{40}Ar$ diagram), MSWD=1.48							11.347	0.080				
$^{40}Ar/^{36}Ar$ intercept							307	16				
sample 129.96–129.97, plagioclase, grain size 0.30–0.50 mm, 34.0 mg, irradiation PAV–64, J=0.0004597±0.0000028												
step-heating data												
*1	0.3 W	14.48	6.168	0.05097	0.3838	4285	10	115	0.1	9.4	30.3	2.7
*2	0.5 W	2.171	16.62	0.01193	0.3622	648.5	16	18	1.1	8.9	86.6	5.4
*3	0.8 W	0.4166	34.79	0.03193	0.6014	131.1	11.0	2.5	6.1	14.8	109.2	6.9
*4	1.3 W	0.04836	24.14	0.00715	0.5783	22.07	11.1	1.2	35.2	14.2	78.8	4.9
*5	2.0 W	0.04464	17.58	0.00511	0.4645	19.61	11.4	1.5	32.7	11.4	71.4	4.5
*6	3.3 W	0.12520	27.29	0.00602	0.8263	49.30	12.3	1.0	24.9	20.3	62.3	3.9
*7	4.3 W	0.01032	12.77	0.00198	0.3562	7.953	11.38	0.81	61.6	8.8	67.6	4.2
*8	10 W	0.01470	28.46	0.00150	0.4904	10.86	10.98	0.98	60.0	12.1	109.5	6.9
Total gas age							12	11				
Error-weighted mean age (8 of 8 steps), MSWD=0.63							11.43	0.46		100.0		

Table S1 Continued

No.	# grains weight (mg) laser power (W)	$^{36}Ar_{(atm)}$	$^{37}Ar_{(Ca)}$	$^{38}Ar_{(Cl)}$	$^{39}Ar_{(K)}$	$^{40}Ar_{(Tot)}$	Age (Ma)	±2σ	$^{40}Ar^{*}$ %	$^{39}Ar_{K}$ %	Ca/K	±2σ
isochron age ($^{36}Ar/^{40}Ar$ vs. $^{39}Ar/^{40}Ar$ diagram), MSWD=0.71							11.39	0.49				
$^{40}Ar/^{36}Ar$ intercept							296.0	2.3				
sample 358.11–358.13, groundmass, grain size 0.30–0.50 mm, 26.0 mg, irradiation PAV–66, J=0.0002761±0.0000011												
step-heating data												
1	0.15 W	0.0425	0.1996	0.00285	0.09441	16.68	21.7	2.5	24.8	0.3	3.99	0.29
2	0.30 W	0.0832	1.864	0.00583	1.610	90.89	20.40	0.18	72.9	5.3	2.19	0.12
3	0.45 W	0.0564	3.460	0.00064	4.745	172.6	16.299	0.089	90.3	15.6	1.376	0.076
*4	0.55 W	0.0247	2.882	0.00050	4.295	145.6	15.965	0.065	95.0	14.1	1.266	0.069
*5	0.70 W	0.0172	2.895	0.00147	4.508	149.4	15.877	0.081	96.6	14.8	1.212	0.066
*6	0.85 W	0.0139	2.193	0.00214	3.617	120.2	15.921	0.062	96.5	11.9	1.144	0.063
*7	1.0 W	0.0122	1.721	0.00084	2.589	86.23	15.830	0.091	95.8	8.5	1.255	0.069
8	1.2 W	0.0158	1.838	0.00257	2.277	76.71	15.691	0.090	93.9	7.5	1.523	0.083
9	1.5 W	0.0283	4.671	0.00515	3.373	113.0	15.381	0.082	92.6	11.1	2.61	0.14
10	2.0 W	0.0187	11.05	0.00524	2.150	71.53	15.23	0.11	92.3	7.1	9.69	0.53
11	3.0 W	0.0046	3.550	0.00045	0.3717	12.73	15.15	0.36	89.2	1.2	18.02	0.99
12	6.0 W	0.0043	1.854	bdl	0.1635	5.915	14.06	0.93	78.3	0.5	21.4	1.3
13	15 W	0.0079	4.921	0.00270	0.6012	21.34	15.68	0.26	89.0	2.0	15.44	0.85
Total gas age							16.08	0.14				
Error-weighted mean age (4 out of 13 steps), MSWD=2.23							15.91	0.14		49.4		
isochron age ($^{36}Ar/^{40}Ar$ vs. $^{39}Ar/^{40}Ar$ diagram), MSWD=1.81							15.74	0.32				
$^{40}Ar/^{36}Ar$ intercept							373	130				
sample 440.83–440.86, feldspars, grain size >0.18 mm, irradiation PAV–66, J=0.0002762±0.0000011												
Total fusion data												
1	1	0.02868	bdl	0.00188	0.8441	935.8	478.1	2.4	99.1	40.3	–	
2	1	0.01993	0.00290	0.00009	0.6835	299.9	202.6	1.8	98.0	32.6	0.008	0.012
*3	1	0.00103	0.00283	0.00020	0.2565	8.701	16.23	0.77	96.5	12.2	0.021	0.034
*4	1	0.00115	0.01055	0.00026	0.2994	10.36	16.60	0.35	96.7	14.3	0.066	0.020
5	1	0.00991	0.04717	0.00008	0.01196	25.48	756	36	88.5	0.6	7.44	0.77
Total gas age							277.7	2.7				
Error-weighted mean age (2 out of 5 runs), MSWD=0.74							16.54	0.34				
sample 564.92–564.93, alkali feldspar, grain size >0.25 mm, irradiation PAV–66, J=0.0002764±0.0000022												
Total fusion data												
*1	1	0.00247	0.03379	0.00024	1.172	41.24	17.15	0.13	98.2	5.6	0.0544	0.0048
*2	1	0.00106	0.00073	0.00011	0.3329	11.81	17.14	0.28	97.3	1.6	0.004	0.018
*3	3	0.00435	0.03915	0.00008	2.150	75.58	17.150	0.071	98.3	10.3	0.0344	0.0036
*4	1	0.00364	0.11080	bdl	1.815	63.64	17.104	0.113	98.3	8.7	0.1152	0.0080
*5	1	0.00252	0.04470	bdl	1.335	46.97	17.19	0.13	98.4	6.4	0.0632	0.0071
*6	1	0.00091	0.01017	bdl	0.6609	22.79	16.91	0.20	98.8	3.2	0.0290	0.0096
*7	3	0.00256	0.01238	0.00036	1.339	47.17	17.20	0.13	98.4	6.4	0.0174	0.0051
*8	3	0.00238	0.01133	bdl	1.021	35.76	17.04	0.14	98.0	4.9	0.0209	0.0062
*9	1	0.00368	0.01569	bdl	0.8246	29.48	17.09	0.14	96.3	3.9	0.0359	0.0065
*10	3	0.00371	0.01851	0.00058	1.438	50.53	17.056	0.098	97.8	6.9	0.0243	0.0049
*11	5	0.00424	0.03978	0.00036	1.776	62.61	17.145	0.092	98.0	8.5	0.0423	0.0044
*12	5	0.00348	0.02656	bdl	2.056	71.95	17.115	0.091	98.5	9.8	0.0244	0.0046
*13	1	0.00213	0.01325	bdl	0.5767	20.59	17.18	0.24	96.9	2.8	0.043	0.012
*14	3	0.00637	0.02152	bdl	1.445	51.64	17.089	0.095	96.3	6.9	0.0281	0.0043

Table S1 Continued

No.	# grains weight (mg) laser power (W)	$^{36}Ar_{(atm)}$	$^{37}Ar_{(Ca)}$	$^{38}Ar_{(Cl)}$	$^{39}Ar_{(K)}$	$^{40}Ar_{(Tot)}$	Age (Ma)	±2σ	$^{40}Ar^*$ %	$^{39}Ar_K$ %	Ca/K	±2σ
*15	3	0.00301	0.02043	0.00020	1.188	41.59	16.999	0.083	97.8	5.7	0.0324	0.0056
*16	3	0.00354	0.02802	bdl	1.789	62.50	17.054	0.085	98.3	8.5	0.0296	0.0034
Total gas age							17.11	0.14				
Error-weighted mean age (16 of 16 runs), MSWD=1.37							17.10	0.14				
isochron age ($^{36}Ar/^{40}Ar$ vs. $^{39}Ar/^{40}Ar$ diagram), MSWD=1.42							17.07	0.17				
$^{40}Ar/^{36}Ar$ intercept							324	86				
sample 640.13–640.16, alkali feldspar, grain size >0.18 mm, irradiation PAV–64, J=0.0004603±0.0000028												
Total fusion data												
*1	1	0.00079	0.00299	bdl	0.3403	7.408	17.42	0.72	96.8	1.4	0.017	0.035
*2	4	0.00099	0.00257	0.00075	1.448	30.78	17.40	0.19	99.0	6.0	0.0033	0.0041
*3	5	0.00225	0.01232	0.00017	1.611	34.48	17.35	0.16	98.0	6.7	0.0144	0.0057
*4	4	0.00506	0.02381	bdl	1.434	31.76	17.44	0.17	95.3	5.9	0.0313	0.0062
*5	5	0.00353	0.00259	0.00095	1.303	28.93	17.69	0.25	96.4	5.4	0.0038	0.0048
*6	5	0.00463	0.01176	bdl	2.389	51.67	17.40	0.13	97.3	9.9	0.0093	0.0030
*7	10	0.00374	0.04596	bdl	3.307	70.53	17.351	0.092	98.4	13.7	0.0262	0.0028
*8	5	0.00131	0.00462	0.00010	1.053	22.57	17.41	0.24	98.2	4.4	0.0083	0.0081
*9	7	0.00217	0.02690	0.00071	1.518	32.49	17.34	0.17	98.0	6.3	0.0334	0.0054
*10	5	0.00217	0.03239	0.00000	1.883	40.26	17.39	0.17	98.4	7.8	0.0325	0.0050
*11	5	0.01272	0.01328	0.00056	1.182	29.33	17.87	0.30	87.2	4.9	0.0212	0.0083
*12	5	0.00238	0.01157	0.00047	1.114	24.02	17.30	0.18	97.0	4.6	0.0196	0.0082
*13	5	0.00101	0.00823	0.00027	1.226	26.13	17.41	0.14	98.8	5.1	0.0127	0.0086
*14	1	0.00120	0.02422	0.00014	0.3461	7.676	17.48	0.67	95.3	1.4	0.132	0.041
*15	6	0.00030	0.01784	0.00074	1.607	33.81	17.34	0.14	99.7	6.7	0.021	0.010
*16	4	0.00150	0.01011	0.00008	0.9866	20.97	17.20	0.26	97.8	4.1	0.019	0.025
*17	7	0.00150	0.01610	bdl	1.385	29.52	17.35	0.16	98.5	5.7	0.022	0.011
Total gas age							17.41	0.11				
Error-weighted mean age (17 of 17 runs), MSWD=1.39							17.39	0.11				
isochron age ($^{36}Ar/^{40}Ar$ vs. $^{39}Ar/^{40}Ar$ diagram), MSWD=0.49							17.30	0.12				
$^{40}Ar/^{36}Ar$ intercept							360	40				
sample 709.14–709.16, alkali feldspar/plagiocalse, grain size >0.18 mm, irradiation PAV–64, J=0.0004614±0.0000028												
Total fusion data												
*1	1	0.03840	0.02621	0.00029	0.4404	21.03	18.21	0.77	46.0	11.8	0.112	0.027
*2	3	0.00232	0.01684	0.00002	1.0655	24.06	18.17	0.24	97.1	28.5	0.030	0.007
*3	3	0.00346	0.10423	0.00151	1.2331	27.91	18.06	0.21	96.3	33.0	0.159	0.012
4	3	0.00950	0.01957	0.00068	0.2263	19.74	61.2	1.7	85.8	6.1	0.163	0.041
5	3	0.00589	0.14108	0.00109	0.1172	4.699	20.9	2.0	63.0	3.1	2.27	0.15
6	3	0.02189	0.15972	0.00088	0.00707	8.645	239	42	25.2	0.2	42.6	5.9
*7	2	0.00442	0.02573	bdl	0.1848	5.517	18.9	1.0	76.3	4.9	0.263	0.063
*8	1	0.00002	0.00377	0.00071	0.1355	3.041	18.5	1.1	99.7	3.6	0.052	0.093
*9	2	0.00194	0.00183	0.00025	0.1204	3.306	18.8	1.2	82.6	3.2	0.029	0.084
10	2	0.00155	0.01106	0.00028	0.2047	5.387	19.93	0.79	91.5	5.5	0.102	0.061
Total gas age							21.47	0.25				
Error-weighted mean age (6 out of 10 runs), MSWD=0.95							18.15	0.18				
isochron age ($^{36}Ar/^{40}Ar$ vs. $^{39}Ar/^{40}Ar$ diagram), MSWD=1.09							18.13	0.20				
$^{40}Ar/^{36}Ar$ intercept							299	12				

Table S1 Continued

No.	# grains weight (mg) laser power (W)	$^{36}Ar_{(atm)}$	$^{37}Ar_{(Ca)}$	$^{38}Ar_{(Cl)}$	$^{39}Ar_{(K)}$	$^{40}Ar_{(Tot)}$	Age (Ma)	±2σ	$^{40}Ar^{*}$ %	$^{39}Ar_{K}$ %	Ca/K	±2σ
sample 709.17–709.19, alkali feldspar/plagioclase, grain size >0.18 mm, irradiation PAV–64, J=0.0004618±0.0000028												
Total fusion data												
*1	1	0.0102	0.0264	0.0004	0.9096	22.61	17.85	0.31	86.6	30.0	0.055	0.009
2	3	0.0060	0.0063	0.0003	0.4819	12.84	19.05	0.56	86.3	15.9	0.025	0.015
3	3	0.0106	0.0926	0.0007	0.4147	12.79	19.29	0.64	75.4	13.7	0.421	0.030
4	3	0.0012	bdl	bdl	0.2186	5.502	19.5	1.0	93.4	7.2	–	
5	4	0.0045	bdl	0.0005	0.0766	10.90	101.3	3.2	87.8	2.5	–	
6	4	0.0134	0.2022	0.0004	0.1640	13.60	48.4	1.6	71.0	5.4	2.33	0.15
*7	2	0.0040	0.0004	0.0004	0.1662	4.957	18.8	1.3	76.2	5.5	0.005	0.087
*8	2	0.0012	0.0032	0.0006	0.2395	5.548	17.99	0.80	93.6	7.9	0.025	0.054
*9	2	0.0012	0.0032	0.0002	0.2607	5.962	17.81	0.79	93.9	8.6	0.023	0.053
*10	2	0.0016	0.0006	bdl	0.09820	2.682	18.6	1.3	82.0	3.2	0.01	0.16
Total gas age							22.26	0.28				
Error-weighted mean age (5 out of 10 runs), MSWD=0.83							17.93	0.28				
isochron age ($^{36}Ar/^{40}Ar$ vs. $^{39}Ar/^{40}Ar$ diagram), MSWD=0.43							17.44	0.86				
$^{40}Ar/^{36}Ar$ intercept							351	92				
sample 831.66–831.68, alkali feldspar, grain size >0.25 mm, irradiation PAV–64, J=0.0004623±0.0000028												
Total fusion data												
*1	1	0.01925	0.00147	bdl	3.252	79.10	18.73	0.12	92.8	13.8	0.0009	0.0024
*2	1	0.00353	0.00523	0.00061	4.039	91.92	18.67	0.09	98.8	17.1	0.0024	0.0023
*3	1	0.00363	0.04793	bdl	1.993	46.04	18.72	0.14	97.6	8.4	0.0454	0.0053
*4	1	0.00303	0.00220	0.00088	1.285	29.75	18.64	0.21	97.0	5.4	0.0032	0.0077
*5	1	0.00232	0.02308	0.00053	1.203	27.98	18.83	0.22	97.5	5.1	0.0362	0.0085
*6	3	0.00246	0.02572	0.00121	1.610	36.80	18.59	0.20	98.0	6.8	0.0301	0.0062
*7	1	0.00456	0.00202	0.00047	1.426	33.33	18.62	0.17	95.9	6.0	0.003	0.011
*8	1	0.00195	bdl	bdl	1.062	24.66	18.82	0.23	97.6	4.5	–	
*9	1	0.00133	0.05870	bdl	1.175	26.89	18.71	0.22	98.5	5.0	0.0943	0.0119
*10	1	0.00131	bdl	0.00053	0.9832	22.57	18.72	0.25	98.2	4.2	–	
*11	1	0.00097	bdl	0.00161	0.8143	18.77	18.83	0.22	98.4	3.5	–	
*12	3	0.00177	0.00090	0.00091	1.668	38.22	18.75	0.15	98.6	7.1	0.0010	0.0144
*13	1	0.00089	0.00330	0.00029	0.4195	9.523	18.32	0.50	97.2	1.8	0.0148	0.0375
*14	3	0.00153	0.00310	0.00019	1.514	34.55	18.69	0.15	98.7	6.4	0.0039	0.0125
*15	3	0.00092	0.00026	0.00004	1.148	26.38	18.88	0.21	98.9	4.9	0.0004	0.0220
Total gas age							18.71	0.12				
Error-weighted mean age (15 of 15 runs), MSWD=0.93							18.71	0.12				
isochron age ($^{36}Ar/^{40}Ar$ vs. $^{39}Ar/^{40}Ar$ diagram), MSWD=0.98							18.69	0.13				
$^{40}Ar/^{36}Ar$ intercept							304	32				
sample 953.28–953.31, alkali feldspar, grain size >0.25 mm, irradiation PAV–64, J=0.0004629±0.0000028												
Total fusion data												
*1	1	0.01191	0.01684	0.00116	5.079	122.5	19.463	0.092	97.1	10.6	0.0063	0.0013
*2	1	0.02354	0.01757	0.00058	4.670	116.2	19.421	0.084	94.0	9.7	0.0071	0.0020
*3	1	0.00596	0.00630	bdl	2.588	62.16	19.39	0.13	97.1	5.4	0.0046	0.0048
*4	1	0.00596	0.05627	bdl	5.929	140.8	19.484	0.079	98.7	12.3	0.0179	0.0020
*5	1	0.00766	0.00982	0.00044	4.105	98.21	19.413	0.091	97.7	8.5	0.0045	0.0019
*6	1	0.00211	0.02411	0.00131	2.135	50.37	19.35	0.14	98.7	4.4	0.0213	0.0057
*7	1	0.00195	0.00975	bdl	2.454	57.92	19.41	0.15	99.0	5.1	0.0075	0.0051
*8	1	0.00200	0.03461	0.00066	2.022	48.02	19.48	0.15	98.7	4.2	0.0323	0.0064

Table S1 Continued

No.	# grains weight (mg) laser power (W)	$^{36}Ar_{(atm)}$	$^{37}Ar_{(Ca)}$	$^{38}Ar_{(Cl)}$	$^{39}Ar_{(K)}$	$^{40}Ar_{(Tot)}$	Age (Ma)	±2σ	$^{40}Ar^{*}$ %	$^{39}Ar_{K}$ %	Ca/K	±2σ
*9	1	0.00371	0.00672	bdl	2.201	52.91	19.56	0.13	97.9	4.6	0.0058	0.0054
*10	1	0.00237	0.00618	0.00111	2.482	59.01	19.51	0.15	98.8	5.2	0.0047	0.0050
*11	1	0.00271	bdl	bdl	2.027	48.07	19.37	0.12	98.3	4.2	–	
*12	5	0.00382	0.03530	bdl	4.360	103.1	19.43	0.10	98.9	9.1	0.0153	0.0028
*13	2	0.00255	0.02238	bdl	3.409	80.63	19.459	0.081	99.0	7.1	0.0124	0.0035
*14	1	0.00169	0.01094	bdl	2.139	50.80	19.53	0.14	99.0	4.5	0.0096	0.0119
*15	1	0.00247	0.02281	0.00052	2.453	57.85	19.34	0.12	98.7	5.1	0.0175	0.0087
Total gas age							19.44	0.12				
Error-weighted mean age (15 of 15 runs), MSWD=1.06							19.44	0.12				
isochron age ($^{36}Ar/^{40}Ar$ vs. $^{39}Ar/^{40}Ar$ diagram), MSWD=1.14							19.45	0.13				
$^{40}Ar/^{36}Ar$ intercept							292	28				
sample 953.54–953.56, alkali feldspar, grain size >0.25 mm, irradiation PAV–64, J=0.0004640±0.0000028												
Total fusion data												
*1	1	0.00865	0.00404	0.00006	0.7982	21.10	19.34	0.31	87.8	5.7	0.010	0.010
*2	1	0.00387	0.00402	bdl	0.8700	21.57	19.55	0.34	94.7	6.2	0.009	0.008
*3	1	0.00113	0.00238	0.00011	1.050	24.95	19.51	0.27	98.6	7.5	0.004	0.013
*4	1	0.01611	0.09551	0.00117	1.095	30.51	19.57	0.25	84.4	7.9	0.164	0.013
*5	2	0.00159	0.00190	0.00011	1.122	26.61	19.39	0.27	98.2	8.1	0.003	0.008
*6	3	0.00474	0.01119	0.00002	2.601	62.66	19.61	0.14	97.7	18.7	0.008	0.003
*7	1	0.00047	0.00007	0.00070	0.5905	14.13	19.73	0.39	99.0	4.2	0.000	0.023
*8	1	0.00242	0.00246	bdl	0.9783	23.62	19.49	0.22	96.9	7.0	0.005	0.016
*9	1	0.00069	0.00080	bdl	0.8507	20.07	19.44	0.21	98.9	6.1	0.002	0.013
*10	2	0.00631	0.00081	bdl	0.9551	24.00	19.30	0.27	92.2	6.9	0.002	0.011
*11	3	0.00431	0.00862	bdl	1.282	31.03	19.33	0.18	95.9	9.2	0.013	0.008
*12	6	0.00509	0.02140	0.00036	1.726	42.06	19.56	0.21	96.4	12.4	0.023	0.012
Total gas age							19.49	0.14				
Error-weighted mean age (12 of 12 runs), MSWD=1.11							19.49	0.14				
isochron age ($^{36}Ar/^{40}Ar$ vs. $^{39}Ar/^{40}Ar$ diagram), MSWD=1.21							19.50	0.15				
$^{40}Ar/^{36}Ar$ intercept							293	23				
sample 1093.00–1093.04, alkali feldspar, grain size >0.25 mm, irradiation PAV–64, J=0.0004645±0.0000028												
Total fusion data												
*1	1	0.00860	0.03536	0.00130	3.273	81.05	19.99	0.12	96.8	4.5	0.0204	0.0043
*2	1	0.03497	0.02248	0.00326	4.290	113.4	20.013	0.092	90.9	5.9	0.0099	0.0012
*3	1	0.04713	0.08456	bdl	5.061	135.3	19.978	0.099	89.7	6.9	0.0315	0.0022
*4	1	0.10761	0.01469	0.00261	2.209	84.89	20.03	0.26	62.5	3.0	0.0125	0.0040
*5	1	0.47887	0.01817	0.00262	3.170	217.8	20.06	0.57	35.0	4.3	0.0108	0.0027
*6	1	0.01003	0.07354	0.00086	3.036	76.26	20.12	0.12	96.1	4.2	0.0457	0.0038
*7	1	0.00489	0.04719	0.00074	3.065	75.19	20.05	0.10	98.0	4.2	0.0290	0.0025
*8	1	0.01018	0.14663	bdl	8.070	196.8	20.008	0.077	98.4	11.1	0.0343	0.0024
9	1	0.02552	0.07371	0.00239	5.054	127.4	19.758	0.093	94.0	6.9	0.0275	0.0023
*10	1	0.02030	0.03709	0.00027	7.233	179.7	20.013	0.091	96.6	9.9	0.0097	0.0016
*11	1	0.00581	0.01489	bdl	2.780	68.47	20.01	0.13	97.5	3.8	0.0101	0.0030
*12	1	0.02047	0.13845	0.00100	5.251	132.4	20.049	0.087	95.4	7.2	0.0497	0.0042
*13	1	0.07014	0.25224	0.00367	5.403	150.1	19.955	0.099	86.2	7.4	0.0881	0.0070
*14	1	0.01867	0.00398	0.00063	3.840	98.34	20.14	0.10	94.4	5.3	0.0020	0.0049
*15	1	0.00191	0.01517	0.00026	1.603	39.07	20.01	0.19	98.5	2.2	0.018	0.011
*16	1	0.00350	0.00540	bdl	2.171	52.86	19.89	0.16	98.0	3.0	0.0047	0.0077

Table S1 Continued

No.	# grains weight (mg) laser power (W)	$^{36}Ar_{(atm)}$	$^{37}Ar_{(Ca)}$	$^{38}Ar_{(Cl)}$	$^{39}Ar_{(K)}$	$^{40}Ar_{(Tot)}$	Age (Ma)	±2σ	$^{40}Ar^{*}$ %	$^{39}Ar_{K}$ %	Ca/K	±2σ
*17	6	0.01137	0.05664	bdl	5.413	132.9	19.938	0.083	97.4	7.4	0.0197	0.0039
*18	1	0.00286	0.00750	0.00046	1.956	47.88	20.04	0.12	98.2	2.7	0.007	0.016
Total gas age							20.00	0.13				
Error-weighted mean age (17 out of 18 runs), MSWD=1.13							20.01	0.12				
isochron age ($^{36}Ar/^{40}Ar$ vs. $^{39}Ar/^{40}Ar$ diagram), MSWD=1.20							20.01	0.13				
$^{40}Ar/^{36}Ar$ intercept							295.4	4.0				

Errors on the single runs are analytical uncertainties. Errors on total gas and error-weighted mean ages also include the unceratinty in *J* value. *, runs used in the weighted mean calculation. bdl, below detection limit